PHYSICAL REVIEW B **95**, 201201(R) (2017)

Semiconductor, topological semimetal, indirect semimetal, and topological Dirac semimetal phases of $Ge_{1-x}Sn_x$ alloys

H.-S. Lan,[1,*] S. T. Chang,[2,†] and C. W. Liu[1,3,4,‡]

[1]*Graduate Institute of Electronics Engineering and Department of Electrical Engineering, National Taiwan University, Taipei 10617, Taiwan*

[2]*Department of Electrical Engineering, National Chung Hsing University, Taichung 40227, Taiwan*

[3]*Graduate Institute of Photonics and Optoelectronics, National Taiwan University, Taipei 10617, Taiwan*

[4]*National Nano Device Labs, Hsinchu 30078, Taiwan*

(Received 8 November 2016; revised manuscript received 31 March 2017; published 5 May 2017)

Electronic structures of $Ge_{1-x}Sn_x$ alloys ($0 \leqslant x \leqslant 1$) are theoretically studied by the nonlocal empirical pseudopotential method. For relaxed $Ge_{1-x}Sn_x$, a topological semimetal is found for $x > 41\%$ with gapless and band inversion at the Γ point, while there is an indirect-direct band-gap transition at $x = 8.5\%$. For strained $Ge_{1-x}Sn_x$ on a Ge substrate, semimetals with a negative indirect band gap appear for $x > 43\%$, and the strained $Ge_{1-x}Sn_x$ on Ge is always an indirect band-gap semiconductor for $x < 43\%$. With appropriate biaxial compressive strains, a topological Dirac semimetal is found with band inversion at Γ and one pair of Dirac cones along the [001] direction.

DOI: 10.1103/PhysRevB.95.201201

Gray tin (α-Sn) is a topological semimetal [1–3] (also referred to as a topological zero-gap semiconductor) due to its inverted Γ_7^- and Γ_8^+ band states at the zone center in reciprocal space, satisfying the nonzero Z_2 topological invariant in the $k_z = 0$ plane [3]. Moreover, a strong topological insulator in strained α-Sn was proposed with an opening gap between the split Γ_8^+ band states (Γ_8^+ and Γ_8^{+*}) at the zone center due to unchanged parity eigenvalues under biaxial strain [3]. A Dirac semimetal [4] with one pair of Dirac cones in the Γ-Z direction in compressively strained α-Sn was also reported [5,6]. Relaxed Ge has the same parity eigenvalues as relaxed α-Sn for the four occupied bands at eight time-reversal invariant momenta (1Γ, $3X$, and $4L$) except for the degenerate Γ_8^+ band states at the zone center [7]. However, if band inversion occurred (Γ_7^- energy level lower than Γ_8^+), the odd parity of Γ_7^- would lead to a nonzero Z_2 invariant. Note that these parity eigenvalues are used to identify the Z_2 invariant, where 0 and 1 for relaxed Ge and α-Sn in the $k_z = 0$ plane, respectively [3]. Recently, diamond structure GeSn alloys have been shown to be attractive for light-emitting [8–10] and electronic [11,12] applications owing to the potential direct band gap of the GeSn alloys and small transport effective masses, respectively. The indirect-direct band-gap transition of relaxed GeSn (r-GeSn) alloys reportedly occurred at a Sn content of around 7%–10% [8,13–16]. A zero-gap behavior was also reported for r-GeSn at a Sn content larger than ~40% based on band-structure calculations [17,18]. However, the occurrence of band inversion in metallic GeSn alloys, implying a nonzero Z_2 invariant in GeSn alloys, has yet to be discussed. The nonlocal empirical pseudopotential method (EPM) has been widely used for calculating the electronic band structures of SiGe [19–21] and GeSn [11,15,22] alloy systems using the virtual crystal approximation (VCA). The pseudocharge density ρ_{pseu} calculated by the electronic wave function was used for determining the bonding characteristics of Ge [23] and α-Sn [24]. Note that the Γ_7^- and Γ_8^+ band states at the zone center are s like (antibonding s orbitals) and p like (bonding p orbitals), respectively, for both Ge and α-Sn [25]. The calculated band gaps and band offsets in strained GeSn/relaxed GeSn using our EPM, where the Sn content $\leqslant$0.3, have been reported [26]. In this Rapid Communication, the phase transition from a semiconductor to a topological semimetal in r-$Ge_{1-x}Sn_x$ alloys ($0 \leqslant x \leqslant 1$) is investigated using EPM. This transition is determined from the corresponding wave functions of Γ_7^- and Γ_8^+ band states at the zone center. For strained $Ge_{1-x}Sn_x$ (s-$Ge_{1-x}Sn_x$) alloys ($0 \leqslant x \leqslant 1$), three phases (semiconductor, indirect semimetal, and topological Dirac semimetal) are found, depending on the Sn content and compressive strain level.

In EPM, the one-electron pseudo-Hamiltonian derived from Ref. [27] has four terms of the kinetic energy, local pseudopotential form factors [$V_{loc}(q)$], nonlocal correction terms [$V_{nloc}(\vec{G},\vec{G}')$], and spin-orbit interactions [$V_{so}(\vec{G},\vec{G}')$]. The $V_{loc}(q)$ versus reciprocal lattice vectors ($q = |G - G'|$) are presented by the expression [19,28]

$$V_{loc}^i(q) = \frac{1}{\Omega^i}\frac{b_1^i\left(q^2-b_2^i\right)}{\exp\left[b_3^i\left(q^2-b_4^i\right)\right]+1}\left[\frac{1}{2}\tanh\left(\frac{b_5^i-q^2}{b_6^i}\right)+\frac{1}{2}\right], \tag{1}$$

where Ω^i is the atomic volume and i denotes the Ge or Sn element. The parameters of b_1^i, b_2^i, b_3^i, and b_4^i are obtained by solving the roots of a system of nonlinear equations with the values of $V_{loc}^i(q)$ at $q^2 = \{3,4,8,11\}(2\pi/a_0^i)^2$. The lattice constants (a_0) at 0 K of Ge (5.652 Å) and Sn (6.482 Å) are calculated using the value at room temperature (RT) [29] and the corresponding thermal expansion coefficients [30]. EPM parameters of $V_{loc}(q)$, spin-orbit interactions (ζ and μ), and a fast cutoff tanh part [28] (b_5^i and b_6^i) of Ge and α-Sn (Table I) are adopted from Refs. [20,22,31,32] with a less than 6% adjustment to reach good agreement with the experimental band gaps of Ge [29,33] and α-Sn [34–36] at low temperature. The parameters of the nonlocal correction terms are obtained from Ref. [27] and the number of the element plane wave

*hslan@ntu.edu.tw, huangsianglan@gmail.com

†stchang@dragon.nchu.edu.tw

‡chee@cc.ee.ntu.edu.tw

TABLE I. Pseudopotential parameters used for Ge and Sn [31].

Parameter	Ge	Sn
$V_{\rm loc}(\sqrt{3})$(Ry)	−0.2351[a]	−0.191
$V_{\rm loc}(\sqrt{4})$(Ry)	−0.1572	−0.152
$V_{\rm loc}(\sqrt{8})$(Ry)	0.0186[a]	−0.008
$V_{\rm loc}(\sqrt{11})$(Ry)	0.055[a]	0.04
ζ (Å^{-1})	5.34	4.75
μ (10^{-4} Ry)	9.4[b]	22.5
b_5 (atomic units)	4.5[a]	3.9[c]
b_6 (atomic units)	0.3[a]	0.3[c]

[a]Reference [32].
[b]Reference [20].
[c]Reference [22].

basis set $\{\vec{G}\}$ is 339. Details of the three terms ($V_{\rm loc}$, $V_{\rm nloc}$, and $V_{\rm so}$) were reported comprehensively by theoretical works [15,19,20,27,31,32,37]. Here, we describe the approaches to take into account both the strain and alloy effects in these three terms. The terms of $V_{\rm loc}$ and $V_{\rm nloc}$, and the parameter λ in the $V_{\rm so}$ of Ge-Sn alloy systems, are obtained by VCA using the following formulas,

$$V^{{\rm Ge}_{1-x}{\rm Sn}_x}(q) = (1-x)\frac{\Omega^{\rm Ge}}{\Omega_{\rm s}^{{\rm Ge}_{1-x}{\rm Sn}_x}}V^{\rm Ge}(q) + x\frac{\Omega^{\rm Sn}}{\Omega_{\rm s}^{{\rm Ge}_{1-x}{\rm Sn}_x}}V^{\rm Sn}(q), \quad (2)$$

both for $V_{\rm loc}$ and $V_{\rm nloc}$,

$$\lambda^{{\rm Ge}_{1-x}{\rm Sn}_x}(K,K') = (1-x)\lambda^{\rm Ge}(K,K') + x\lambda^{\rm Sn}(K,K'). \quad (3)$$

The $\{\vec{G}\}$ and the normalizing strained atomic volume Ω_s^i generated from the lattice vectors are considered in the Hamiltonian matrix [20] with the strain and alloy effects. The linear interpolation of the elastic constants (C_{11}, C_{12}, and C_{44}) [38] and a bowing of 0.047 Å [39] for the lattice constant of GeSn alloys are used. Note that the coherent potential approximation (CPA) that is in agreement with the VCA results in homogeneous GeSn alloys (substitutional α-Sn in Ge) was reported in Refs. [40,41]. CPA was used to consider the inhomogeneous GeSn alloys with β-Sn defects that may not exist at 0 K discussed in this work according to the formula in Ref. [41].

The band structure of r-$Ge_{0.65}Sn_{0.35}$ [Fig. 1(a)], a typical direct-gap semiconductor, owns the conduction band edge at the zone center (Γ_7^- state) and the degenerate valence band edges (Γ_8^+ states for heavy hole and light hole bands) with a band gap of ∼70 meV. However, the band structure of r-$Ge_{0.55}Sn_{0.45}$ [Fig. 1(b)] shows a gapless topological semimetal behavior with degenerate Γ_8^+ states above the Γ_7^- state. The corresponding constant $\rho_{\rm pseu}$ contours around the two atoms in the unit cell of the band states of s-like Γ_7^- and p-like Γ_8^+ show the band inversion of r-$Ge_{0.55}Sn_{0.45}$ as compared to r-$Ge_{0.65}Sn_{0.35}$ [Figs. 1(c) and 1(d)]. The band inversion leads to a nonzero Z_2 invariant, referred to as the topological behavior. The same parity eigenvalues of r-$Ge_{0.55}Sn_{0.45}$ as r-Sn for the four occupied bands at eight time-reversal invariant momenta are confirmed using our EPM. Without spin-orbit coupling (SOC), the parity inversion in r-$Ge_{0.55}Sn_{0.45}$ disappears.

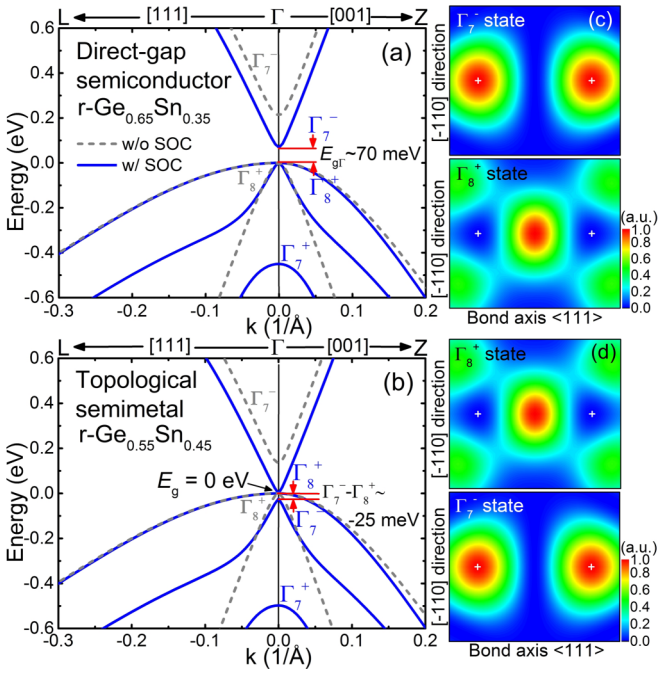

FIG. 1. The calculated band structures with and without spin-orbit coupling (SOC) around the zone center of (a) a direct-gap semiconductor (r-$Ge_{0.65}Sn_{0.35}$) and (b) a gapless topological semimetal (r-$Ge_{0.55}Sn_{0.45}$). The constant pseudocharge density ($\rho_{\rm pseu}$) contours of the two atoms (indicated by +) in the unit cell of (c) r-$Ge_{0.65}Sn_{0.35}$ and (d) r-$Ge_{0.55}Sn_{0.45}$ to identify s-like Γ_7^- and p-like Γ_8^+.

The calculated indirect band gap ($E_{gL} = L_6^+ - \Gamma_8^+$), direct band gap ($E_{g\Gamma} = \Gamma_7^- - \Gamma_8^+$), and $E_{g\Gamma}$ + spin-orbit splitting (Δ_0) ($E_{g\Gamma} + \Delta_0 = \Gamma_7^- - \Gamma_7^+$) as a function of Sn content for r-$Ge_{1-x}Sn_x$ are shown in Fig. 2. Our calculations agree well with the reported experimental data at low Sn content ($E_{g\Gamma}$ and $E_{g\Gamma} + \Delta_0$) near 0 K [14,42]. The calculated band gaps of α-Sn ($E_{gL} = 0.13$ eV, $E_{g\Gamma} = -0.43$ eV, and

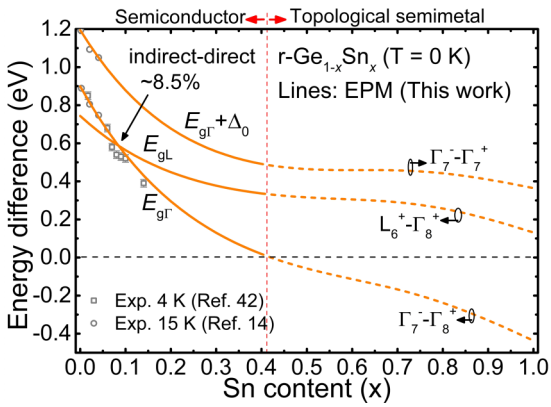

FIG. 2. The calculated energy differences of $\Gamma_7^- - \Gamma_8^+$, $L_6^+ - \Gamma_8^+$, and $\Gamma_7^- - \Gamma_7^+$ as a function of Sn content as compared with the reported experimental data [14,42]. The solid lines indicate the semiconductor band gaps including E_{gL}, $E_{g\Gamma}$, and $E_{g\Gamma} + \Delta_0$, and the dashed lines ($x > 41\%$) indicate the energy differences of the topological semimetal.

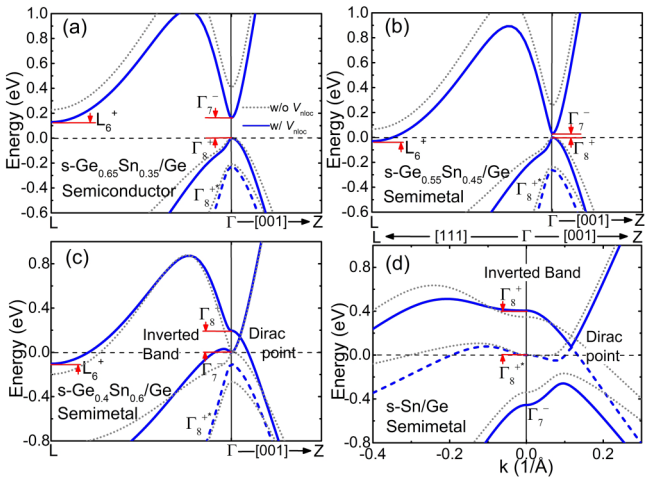

FIG. 3. Electronic band structures of s-$Ge_{1-x}Sn_x$ on Ge with different Sn content with and without a nonlocal potential ($V_{\rm nloc}$). (a) An indirect-gap semiconductor (s-$Ge_{0.65}Sn_{0.35}$ on Ge). (b) An indirect semimetal (s-$Ge_{0.55}Sn_{0.45}$ on Ge). (c) An indirect semimetal with the inverted band at the zone center and a Dirac point along the [001] direction (s-$Ge_{0.4}Sn_{0.6}$). (d) An indirect semimetal with the inverted band at the zone center and a Dirac point along the [001] direction (s-Sn on Ge). Note that the opening gap at zone center is $\Gamma_8^+ - \Gamma_7^-$ and $\Gamma_8^+ - \Gamma_8^{+*}$ for (c) and (d), respectively.

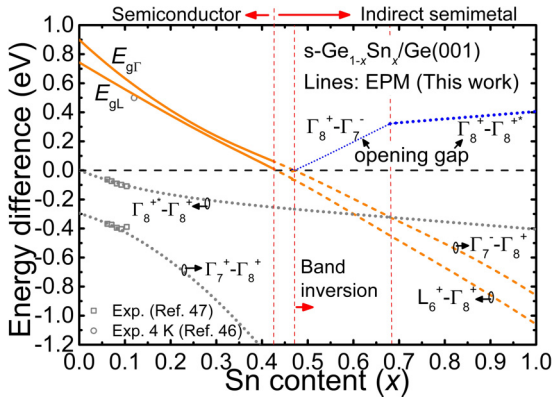

FIG. 4. The calculated energy differences of $\Gamma_7^- - \Gamma_8^+$, $L_6^+ - \Gamma_8^+$, $\Gamma_8^{+*} - \Gamma_8^+$, and $\Gamma_7^+ - \Gamma_8^+$ of s-$Ge_{1-x}Sn_x$ on Ge as a function of Sn content as compared with the reported experimental data [46,47]. A semiconductor to indirect semimetal transition is found at $x > 43\%$ and the band inversion at the zone center occurs at $x > 47\%$. The opening gap at the zone center changes from $\Gamma_8^+ - \Gamma_7^-$ to $\Gamma_8^+ - \Gamma_8^{+*}$ at $x \sim 68\%$.

$\Delta_0 = 0.8$ eV) are also consistent with reported values ($E_{gL} = 0.12$ eV [34,36], $E_{g\Gamma} = -0.42$ eV [35], and $\Delta_0 = 0.8$ eV [35]). There are no experimental E_{gL} data of r-$Ge_{1-x}Sn_x$ near 0 K reported in the literature. $E_{g\Gamma}$ decreases faster than E_{gL} with increasing Sn content and this results in an indirect-direct band-gap transition around $x = 8.5\%$ for r-$Ge_{1-x}Sn_x$ [26]. For $x > 41\%$, the degenerate Γ_8^+ forms a gapless topological semimetal ($E_g = 0$ eV) with the band inversion. The s-like Γ_7^- falls below the two p-like Γ_8^+ states in energy, i.e., $\Gamma_7^- - \Gamma_8^+ \sim -25$ meV of r-$Ge_{0.55}Sn_{0.45}$ [Fig. 1(b)]. The energy differences of $\Gamma_7^- - \Gamma_8^+$, $L_6^+ - \Gamma_8^+$, and $\Gamma_7^- - \Gamma_7^+$ in gapless r-$Ge_{1-x}Sn_x$ alloys are also shown in Fig. 2 for comparison.

For an s-$Ge_{1-x}Sn_x$ layer on a Ge (001) substrate, the phase transition in the band structure from a semiconductor to indirect semimetal with an increase of Sn content is shown in Fig. 3. Note that we assume that a metastable fully strained thin layer s-$Ge_{1-x}Sn_x$ could be grown on Ge even though a high Sn content of s-$Ge_{1-x}Sn_x$ on Ge ($x > 46\%$) is still under investigation [43,44]. The s-$Ge_{0.65}Sn_{0.35}$ on Ge [Fig. 3(a)] has a typical indirect band gap with conduction band edges at the L_6^+ states and the valence band edge at the Γ_8^+ state (the heavy hole band). For s-$Ge_{0.55}Sn_{0.45}$ on Ge [Fig. 3(b)], the L_6^+ states fall below the Γ_8^+ state, resulting in an indirect semimetal with a negative indirect band gap ($L_6^+ - \Gamma_8^+ \sim -30$ meV). As the Sn content reaches to 60% [Fig. 3(c)], the band inversion of the Γ_7^- and Γ_8^+ states occurs at the zone center with an opening gap ($\Gamma_8^+ - \Gamma_7^-$) at the Γ point and a Dirac point along the [001] direction, but the L_6^+ states are still at the conduction band minimum. In this case, s-$Ge_{0.4}Sn_{0.6}$ on Ge is referred to as an indirect semimetal with a negative indirect band gap (not a topological Dirac semimetal) owing to the uncertainly occupied Γ_7^- state with respect to the unknown Fermi energy [6]. For s-Sn on Ge in Fig. 3(d), the large compressive strain ($\sim -12.8\%$) moves the Γ_8^{+*} state upwards beyond the Γ_7^- state. However, the conduction band edges remain at the L_6^+ states. Moreover, the Dirac points are along the [001] direction, not along the [100] or [010] direction on the compressively strained plane, which is consistent with a previous report [45]. Without the energy dependence the $V_{\rm nloc}$ term for the core states, the symmetries allow for the occurrences of band inversion and the Dirac point even though there is a loss of accuracy in energy. The coexistence of band inversion and a Dirac point in s-$Ge_{0.4}Sn_{0.6}$ on Ge without $V_{\rm nloc}$ is shown in Fig. 3(c).

Figure 4 shows detailed phase transitions in s-$Ge_{1-x}Sn_x$ on Ge as a function of Sn content. The calculated energies, E_{gL}, $\Gamma_8^{+*} - \Gamma_8^+$, and $\Gamma_7^+ - \Gamma_8^+$, of s-$Ge_{1-x}Sn_x$ on Ge are consistent with reported experimental data [46,47] at low Sn content. For $0 \leqslant x \leqslant 30\%$, $E_{g\Gamma}$ decreases faster than E_{gL}. As a result, the energy difference $E_{g\Gamma} - E_{gL}$ decreases with increasing Sn content. However, no crossover point is found because the increasing biaxial compressive strain with increasing Sn content moves the Γ_7^- state upwards as compared to the L_6^+ states, and thus the difference ($E_{g\Gamma} - E_{gL}$) increases again for $x > \sim 30\%$. An indirect semimetal with a negative indirect band gap, $L_6^+ - \Gamma_8^+$, occurs for $x > 43\%$. The band inversion at the zone center is found for $x > 47\%$, and the opening gap at the zone center changes from $\Gamma_8^+ - \Gamma_7^-$ to $\Gamma_8^+ - \Gamma_8^{+*}$ at $x \sim 68\%$ due to the upward movement of Γ_8^{+*} energy beyond the Γ_7^- state with increasing biaxial compressive strain.

In order to form a topological Dirac semimetal in s-$Ge_{1-x}Sn_x$, the biaxial compressive strain should be smaller than that of s-$Ge_{1-x}Sn_x$ on Ge to make the energy of the L_6^+ states in Figs. 3(b) and 3(c) beyond the Γ_8^+ state. In this case, the Fermi energy lies in the middle of the Dirac points to ensure the occupied Γ_7^- state [3,6]. In the phase diagram defined by the Sn content ($0 \leqslant x \leqslant 1$) and biaxial compressive strain ($0.1\% \leqslant |\varepsilon_{||}| \leqslant 3.5\%$) [Fig. 5(a)], the semiconductor/topological Dirac semimetal transition for s-$Ge_{1-x}Sn_x$ is found in the Sn content range of 41%–60% [the red line in Fig. 5(a)]. For the semiconductor phase, the

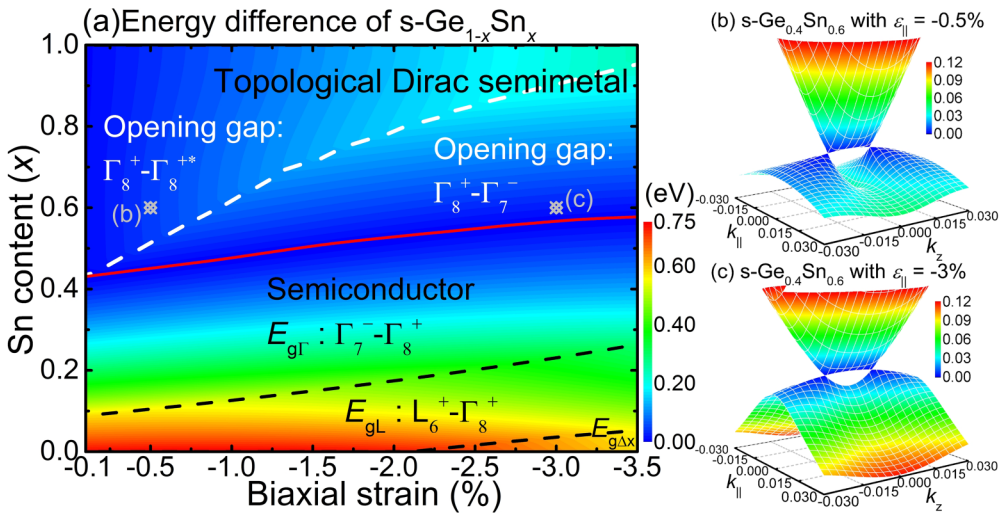

FIG. 5. (a) The phase diagram as a function of Sn content ($0 \leqslant x \leqslant 1$) and biaxial compressive strain ($0.1\% \leqslant |\varepsilon_{||}| \leqslant 3.5\%$). The red line indicates the phase transition between the direct-gap semiconductor and topological Dirac semimetal. The black dashed lines distinguish the three regions for the fundamental band gap ($E_{g\Delta x}$, E_{gL}, and $E_{g\Gamma}$) of the semiconductor. The white dashed line distinguishes the two regions for the opening gap ($\Gamma_8^+ - \Gamma_8^{+*}$ and $\Gamma_8^+ - \Gamma_7^-$) at the zone center of the topological Dirac semimetal. The band structure on the $k_{||}$-k_z plane has one pair of three-dimensional Dirac cones located along the k_z direction for s-$Ge_{0.4}Sn_{0.6}$ with (b) the biaxial compressive strain ($\varepsilon_{||}$) of -0.5% and (c) the biaxial compressive strain ($\varepsilon_{||}$) of -3%. The opening gap in (b) is $\Gamma_8^+ - \Gamma_8^{+*}$, while the opening gap in (c) is $\Gamma_8^+ - \Gamma_7^-$.

fundamental band gap has three distinct regions for $E_{g\Delta x}$, E_{gL}, and $E_{g\Gamma}$. Note that the conduction band minima at Δ points are split into the fourfold ($2\Delta_x$ and $2\Delta_y$) and twofold ($2\Delta_z$) valley degeneracies under biaxial compressive strain and the fourfold has lower energy than the twofold. The band structures on the $k_{||}$-k_z plane of s-$Ge_{0.4}Sn_{0.6}$ with a biaxial compressive strain ($\varepsilon_{||}$) of -0.5% and -3% show one pair of three-dimensional Dirac cones along the k_z direction [Figs. 5(b) and 5(c)] and the band inversion at the zone center. Note that the $k_{||}$ direction refers to the k_x [100] or k_y [010] axis perpendicular to the k_z [001] direction. The nonzero Z_2 topological invariants in the $k_z = 0$ plane of s-$Ge_{0.4}Sn_{0.6}$ with $\varepsilon_{||} = -0.5\%$ and -3% are also confirmed by the parity eigenvalues of the four occupied bands using our EPM. This is classified as a topological Dirac semimetal. [4] In addition, the effective Hamiltonian for the Dirac fermion [4] is used to obtain the velocity along the $k_{||}$ direction of 8.35×10^6 and 1.45×10^7 cm^2/s for s-$Ge_{0.4}Sn_{0.6}$ with $\varepsilon_{||} = -0.5\%$ and -3%, respectively. The opening gap at the zone center of the topological Dirac semimetal changes from $\Gamma_8^+ - \Gamma_8^{+*}$ to $\Gamma_8^+ - \Gamma_7^-$ [the white dashed line in Fig. 5(a)] with increasing biaxial compressive strain due to the Γ_7^- energy beyond the Γ_8^{+*} state under high strain level.

Semiconductors with a direct or indirect band gap, indirect semimetals with a negative indirect band gap, topological semimetals, and topological Dirac semimetals are found in $Ge_{1-x}Sn_x$ alloy systems by band-structure calculations using nonlocal EPM. The Sn content and strain level determine the phase of $Ge_{1-x}Sn_x$. The existence of diverse phases in $Ge_{1-x}Sn_x$ alloys has encouraged the exploration of possible phenomena such as chirality, and applications of GeSn alloys.

This work was supported by Ministry of Science and Technology, Taiwan, R.O.C. under Grants No. 105-2622-8-002-001-, No. 105-2911-I-009-301, and No. 103-2221-E-002-232-MY3. The support of high-performance computing facilities by the Computer and Information Networking Center, National Taiwan University, is also highly appreciated.

[1] H. Lin, T. Das, Y. J. Wang, L. A. Wray, S.-Y. Xu, M. Z. Hasan, and A. Bansil, Phys. Rev. B **87**, 121202(R) (2013).
[2] J. Vidal, X. Zhang, V. Stevanović, J.-W. Luo, and A. Zunger, Phys. Rev. B **86**, 075316 (2012).
[3] L. Fu and C. L. Kane, Phys. Rev. B **76**, 045302 (2007).
[4] B.-J. Yang and N. Nagaosa, Nat. Commun. **5**, 4898 (2014).
[5] V. A. Rogalev, T. Rauch, M. R. Scholz, F. Reis, L. Dudy, A. Fleszar, M.-A. Husanu, V. N. Strocov, J. Henk, I. Mertig, J. Schäfer, and R. Claessen, Phys. Rev. B **95**, 161117(R) (2017).
[6] H. Huang and F. Liu, arXiv:1612.00987.
[7] M. L. Cohen and J. Chelikowsky, *Electronic Structure and Optical Properties of Semiconductors*, 2nd ed., Springer Series in Solid-State Sciences Vol. 75 (Springer, Berlin, 1989).
[8] S. Wirths, R. Geiger, N. von den Driesch, G. Mussler, T. Stoica, S. Mantl, Z. Ikonic, M. Luysberg, S. Chiussi, J. M. Hartmann, H. Sigg, J. Faist, D. Buca, and D. Grtzmacher, Nat. Photon. **9**, 88 (2015).
[9] H. S. Mączko, R. Kudrawiec, and M. Gladysiewicz, Sci. Rep. **6**, 34082 (2016).
[10] C.-Y. Lin, C.-H. Huang, S.-H. Huang, C.-C. Chang, C. W. Liu, Y.-C. Huang, H. Chung, and C.-P. Chang, Appl. Phys. Lett. **109**, 091103 (2016).
[11] H.-S. Lan and C. W. Liu, Appl. Phys. Lett. **104**, 192101 (2014).
[12] Y.-C. Yeo, X. Gong, M. J. H. van Dal, G. Vellianitis, and M. Passlack, in *2015 IEEE International Electron Devices Meeting (IEDM), Technical Digest* (IEEE, New York, 2016), p. 2.4.1.

[13] J. D. Gallagher, C. L. Senaratne, J. Kouvetakis, and J. Menndez, Appl. Phys. Lett. **105**, 142102 (2014).
[14] V. R. D'Costa, C. S. Cook, A. G. Birdwell, C. L. Littler, M. Canonico, S. Zollner, J. Kouvetakis, and J. Menéndez, Phys. Rev. B **73**, 125207 (2006).
[15] K. L. Low, Y. Yang, G. Han, W. Fan, and Y.-C. Yeo, J. Appl. Phys. **112**, 103715 (2012).
[16] F. L. Freitas, J. Furthmüller, F. Bechstedt, M. Marques, and L. K. Teles, Appl. Phys. Lett. **108**, 092101 (2016).
[17] D. W. Jenkins and J. D. Dow, Phys. Rev. B **36**, 7994 (1987).
[18] M.-H. Lee, P.-L. Liu, Y.-A. Hong, Y.-T. Chou, J.-Y. Hong, and Y.-J. Siao, J. Appl. Phys. **113**, 063517 (2013).
[19] M. V. Fischetti and S. E. Laux, J. Appl. Phys. **80**, 2234 (1996).
[20] M. M. Rieger and P. Vogl, Phys. Rev. B **48**, 14276 (1993).
[21] P. Vogl, M. M. Rieger, J. A. Majewski, and G. Abstreiter, Phys. Scr. **1993**, 476 (1993).
[22] S. Gupta, B. Magyari-Köpe, Y. Nishi, and K. C. Saraswat, J. Appl. Phys. **113**, 073707 (2013).
[23] J. P. Walter and M. L. Cohen, Phys. Rev. B **4**, 1877 (1971).
[24] H. Aourag, B. Soudini, B. Khelifa, and A. Belaidi, Phys. Status Solidi B **161**, 685 (1990).
[25] P. Y. Yu and M. Cardona, *Fundamentals of Semiconductors*, 3rd ed. (Springer, Berlin, 2001).
[26] H.-S. Lan and C. W. Liu, J. Phys. D: Appl. Phys. **50**, 13LT02 (2017).
[27] J. R. Chelikowsky and M. L. Cohen, Phys. Rev. B **14**, 556 (1976).
[28] P. Friedel, M. S. Hybertsen, and M. Schluter, Phys. Rev. B **39**, 7974 (1989).
[29] S. Adachi, *Properties of Group-IV, III-V and II-VI Semiconductors* (Wiley, Hoboken, NJ, 2005).
[30] R. Roucka, Y.-Y. Fang, J. Kouvetakis, A. V. G. Chizmeshya, and J. Menéndez, Phys. Rev. B **81**, 245214 (2010).
[31] W. Potz and P. Vogl, Phys. Rev. B **24**, 2025 (1981).
[32] J. Kim and M. V. Fischetti, J. Appl. Phys. **108**, 013710 (2010).
[33] S. Zwerdling, B. Lax, L. M. Roth, and K. J. Button, Phys. Rev. **114**, 80 (1959).
[34] R. F. C. Farrow, D. S. Robertson, G. M. Williams, A. G. Cullis, G. R. Jones, I. M. Young, and P. N. J. Dennis, J. Cryst. Growth **54**, 507 (1981).
[35] T. Brudevoll, D. S. Citrin, M. Cardona, and N. E. Christensen, Phys. Rev. B **48**, 8629 (1993).
[36] R. J. Wagner and A. W. Ewald, J. Phys. Chem. Solids **32**, 697 (1971).
[37] P. Harrison, *Quantum Well, Wires and Dots*, 2nd ed. (Wiley, Hoboken, NJ, 2005), pp. 373–379.
[38] G.-E. Chang, S.-W. Chang, and S. L. Chuang, IEEE J. Quantum Electron. **46**, 1813 (2010).
[39] R. Beeler, R. Roucka, A. V. G. Chizmeshya, J. Kouvetakis, and J. Menendez, Phys. Rev. B **84**, 035204 (2011).
[40] J. D. Querales-Flores, C. I. Ventura, J. D. Fuhr, and R. A. Barrio, J. Appl. Phys. **120**, 105705 (2016).
[41] C. I. Ventura, J. D. Fuhr, and R. A. Barrio, Phys. Rev. B **79**, 155202 (2009).
[42] H. Pérez Ladrón de Guevara, A. G. Rodrguez, H. Navarro-Contreras, and M. A. Vidal, Appl. Phys. Lett. **91**, 161909 (2007).
[43] A. Suzuki, O. Nakatsuka, S. Shibayama, M. Sakashita, W. Takeuchi, M. Kurosawa, and S. Zaima, Appl. Phys. Lett. **107**, 212103 (2015).
[44] A. Suzuki, O. Nakatsuka, S. Shibayama, M. Sakashita, W. Takeuchi, M. Kurosawa, and S. Zaima, Jpn. J. Appl. Phys. **55**, 04EB12 (2016).
[45] A. Barfuss, L. Dudy, M. R. Scholz, H. Roth, P. Höpfner, C. Blumenstein, G. Landolt, J. H. Dil, N. C. Plumb, M. Radovic, A. Bostwick, E. Rotenberg, A. Fleszar, G. Bihlmayer, D. Wortmann, G. Li, W. Hanke, R. Claessen, and J. Schäfer, Phys. Rev. Lett. **111**, 157205 (2013).
[46] D. Stange, S. Wirths, N. von den Driesch, G. Mussler, T. Stoica, Z. Ikonic, J. M. Hartmann, S. Mantl, D. Grützmacher, and D. Buca, ACS Photonics **2**, 1539 (2015).
[47] K. Zelazna, M. P. Polak, P. Scharoch, J. Serafinczuk, M. Gladysiewicz, J. Misiewicz, J. Dekoster, and R. Kudrawiec, Appl. Phys. Lett. **106**, 142102 (2015).